Hindawi
International Journal of Energy Research
Volume 2023, Article ID 4440117, 10 pages
https://doi.org/10.1155/2023/4440117

Research Article

$CuFeO_2$/Cu Photoelectrode Modified with SrTiO3 Perovskite for Efficient Hydrogen Generation from Sanitation Water

Aya Ahmed,[1,2] Ashour M. Ahmed,[3] Ahmed A. Abdel-Khaliek,[1] Mohamed Shaban,[4] Ahmed Adel A. Abdelazeez,[5] and Mohamed Rabia[2,6]

[1]*Physical Chemistry Laboratory, Chemistry Department, Faculty of Science, Beni-Suef University, Beni-Suef 62514, Egypt*
[2]*Nanophotonics and Applications Lab, Physics Department, Faculty of Science, Beni-Suef University, Beni-Suef 62514, Egypt*
[3]*Physics Department, College of Science, Imam Mohammad Ibn Saud Islamic University (IMSIU), Riyadh 11623, Saudi Arabia*
[4]*Physics Department, Faculty of Science, Islamic University of Madinah, Madinah, Saudi Arabia*
[5]*Nanoscale Science, Chemistry Department, University of North Carolina at Charlotte, Charlotte, NC 28223, USA*
[6]*Nanomaterials Science Research Laboratory, Chemistry Department, Faculty of Science, Beni-Suef University, Beni-Suef, Egypt*

Correspondence should be addressed to Ahmed Adel A. Abdelazeez; aabdelh2@uncc.edu
and Mohamed Rabia; mohamedchem@science.bsu.edu.eg

Received 15 March 2023; Revised 27 May 2023; Accepted 4 July 2023; Published 28 July 2023

Academic Editor: Tholkappiyan Ramachandran

We prepared a perovskite material, copper-doped strontium titanate (Cu-$SrTiO_3$), using the chemical bath deposition method and cast it on a $CuFeO_2$/Cu photoelectrode to generate hydrogen from sanitation water splitting. This preparation method considers a simple mass product and does not depend on complex techniques. The prepared perovskite materials had a compact nano-/microstructure. Both $CuFeO_2$ and Cu-$SrTiO_3$/$CuFeO_2$ exhibited excellent optical properties, with bandgap values of 1.4 and 1.26 eV, respectively. Here, the prepared $CuFeO_2$ and Cu-$SrTiO_3$ thin films are used as photoelectrodes for hydrogen generation, and their current-voltage relationship is analyzed under various conditions, such as different light intensities, wavelengths, and temperatures. This approach is promising for using wastewater as a source of hydrogen gas without requiring any additional electrolyte, making it a dual-purpose approach for both hydrogen generation and wastewater treatment. Through the electrochemical study, increasing the light intensity from 25 to 100 $mW.cm^{-2}$ resulted in a corresponding increase in the produced J_{ph} values from -1.02 to -1.292 $mA.cm^{-2}$. Similarly, the J_{ph} values increased from -1.25 to -1.91 $mA.cm^{-2}$ as the temperature increased from 30 to 70°C. We also calculated all thermodynamic parameters, the quantum efficiency (QE), and incident photon to current conversion efficiency (IPCE). For the Cu-$SrTiO_3$/$CuFeO_2$/Cu photoelectrode, the activation energy (E_a) value was 14.14 kJ mol^{-1}, while the ΔH^* and ΔS^* values were 11.46 $kJ{\cdot}mol^{-1}$ and 34.9 $kJ^{-1}{\cdot}mol^{-1}$, respectively. Additionally, the IPCE value was 3.31%. The prepared photoelectrode showed high stability and low cost, making it a potential candidate for industrial applications.

1. Introduction

Renewable energy sources are critical to human life's actuality. The bulk of these sources are based on photocatalytic materials used in the fabrication of photodetectors, solar cells, and photocatalytic electrodes [1–4]. Hydrogen is one of the most ecofriendly and sustainable energy carriers available, and it may replace fossil fuels. Currently, most of the H_2 is generated from methane or fossil fuels with a significant carbon footprint. Extensive research is being performed to develop new technologies for economically producing hydrogen from renewable materials [5–7]. Photoelectrochemical (PEC) water splitting is regarded as one of the most promising methods for hydrogen production. The creation of H_2 gas by a water-splitting process is a vital energy source for aircraft, vehicles, and industries that utilize H_2 fuel. The synthesized photoelectrode must have high water-splitting efficiency and qualities that qualify it for numerous applications, such as low cost, simple preparation, easy operation, and stability [8]. The electrode can be utilized in sunlight

or with another type of artificial light. Perovskite oxide substances are currently considered promising photocatalysts for a variety of potential photocatalytic applications due to their promising qualities, including compositional flexibility, excellent electronic, optical, and magnetic properties, overall resistance to photocorrosion, and excellent thermal stability properties [6, 9]. These characteristics are anticipated to improve their stability and desired photocatalytic activity. The single perovskite oxides can be represented as ABO_3, where A and B are metal cations. Alkaline-earth metal cations, transition metal cations, or alkali metal cations are the three options for A and B [10–12].

The morphologies and surface properties of several perovskite oxides, including $SrTiO_3$, $KTaO_3$, $NaTaO_3$, $KNbO_3$, $Zn_{1-x}Ba_xFe_2O_4$, $ZnFe_{1.96}La_{0.04}O_4$, $BiFeO_3$, and $NaNbO_3$, were observed to have a significant impact on the photocatalytic activities in this context [13–15]. The main characteristics of perovskite oxide-based photocatalysts in solar-driven photocatalytic hydrogen evolution reaction (HER) have been particularly emphasized in several great academic studies over the past few years. Recent studies have proven the insertion of transition metal causes additional enhancement in these perovskite materials that appear as enhancements in the optical and electrical properties [16–20].

Recent advances in single perovskite oxide ABO_3-based photocatalysts, perovskite materials, and SrTiO3-based photocatalysts for use in HER via water splitting were also discussed [21]. Certainly, photocatalysts based on perovskite oxide will play a vital role in solar-driven HER during the next years. It is found that the current H_2 evolution rate is still low and will require further enhancement in the future. This has motivated the scientific community to focus on understanding the existing state of affairs and ideas for improving the overall quality, productivity, and efficiency of perovskite material or oxide catalysts for HER [22–24].

The main goal of this study was to develop a $SrTiO_3$/$CuFeO_2$/Cu photoelectrode for hydrogen generation through water splitting. To achieve this, the $CuFeO_2$ and Cu-$SrTiO_3$ layers were fabricated using combustion and chemical bath deposition methods, respectively. The efficiency of the photoelectrode for H_2 production was evaluated by analyzing its current-voltage relationship under various light intensities, wavelengths, and temperatures. Additionally, various thermodynamic parameters were calculated along with quantum efficiency (QE) and incident photon-to-current conversion efficiency (IPCE). The photoelectrode showed high stability and has promising potential for utilization in the industrial sector.

2. Experimental Methodology

2.1. Preparing of $CuFeO_2$ Perovskite Layer. Cu foil with a 10 mm × 5 mm dimension was immersed in 3 ml of Conc. H_2SO_4 for 15 min on each side, then washed with deionized water. Then, the copper substrate was immersed in 0.1 $FeCl_3$, dissolved in 50 ml of deionized water for 20 min on each side, left hanging to dry in the air for 15 min, then heated over a hot plate at 50°C for 10 min, and then annealed inside a tube at 500°C for 10 min using a CVD furnace.

2.2. Preparation of Cu-$SrTiO_3$ Perovskite Layer. 0.1 M of strontium chloride ($SrCl_2$, 99.6%) and 0.02 M of copper chloride ($CuCl_2$, 99.7%) were dissolved in 10 ml of isopropanol (99.0%) using ultrasonic for 1 min. Then 5 ml of this solution was added to 0.1 M of titanium isopropoxide (99.9%). Cast 100 μl of Cu-$SrTiO_3$ solution over the $CuFeO_2$ layer, then let it dry in the air and then over a hot plate at 50°C for 15min, and then anneal inside a tube at 500°C for 10 min using a CVD furnace. Ag paste is diluted by adding a couple of drops of acetone (98.9%), then deposited on one side of the cell drop using cotton bud and then dried it over a hot plate at 70°C for 2 min.

2.3. Samples Characterization. The prepared perovskite layers were characterized using different devices. The chemical structure was confirmed using an X-ray diffractometer (XRD, Bruker/Siemens D5000, Aubrey, TX, USA) by Kα radiation of Cu (λ = 1.5405 Å) at 30 mA and 40 kV. Moreover, the chemical structure was confirmed using X-ray photoelectron spectroscopy (XPS) models (advance diffractometer, Bruker D8) and K-ALPHA, USA. Besides, the elements inside the materials and morphologies were determined using a scanning electron microscope (SEM, Auriga Zeiss FIB, Zeiss Company, Oberkochen, Germany). Also, the morphologies were confirmed using transmitted electron microscope (TEM) models Hitachi, S-4800, and JEOL JEM-2100, respectively. The optical properties were characterized using a double-beam spectrophotometer (Perkin Elmer Lambda 950, Perkin Elmer Company, Waltham, MA 02451, USA).

2.4. Water-Splitting Test. The water splitting reaction happened under a solar simulator from a three-electrode cell, in which the Cu-$SrTiO_3$/$CuFeO_2$/Cu represented the working electrode as a cathode, whereas graphite and calomel electrodes were worked as counter and reference electrodes, respectively. These electrodes are partially immersed in 30 ml of filtered sanitation water (third-stage treated, company of drinking water and wastewater, Beni-Suef City, Egypt). The measurements were carried out using an electrochemical workstation (CHI660E) at a scan rate of 100 $mV.s^{-1}$. The effects of light intensity (100 to 400 $mW.cm^{-2}$), incident wavelength (390 to 636 nm), temperature reaction (30 to 70°C), and time stability were studied for water splitting for H_2 generation (Figure 1).

3. Results and Discussion

3.1. Analyses

3.1.1. XRD and XPS Analyses. The XRD of the delafossite, $CuFeO_2$, materials are shown in Figure 2 (black line). From this figure, all characteristic peaks related to $CuFeO_2$ are confirmed; this is related to the peaks located at 34.1°, 35.5°, 38.5°, 53°, 61.2°, and 68°. These peaks are matched with the analysis for the hexagonal and rhombohedral structures (JCPDS No. 75-2146) [25]. These peaks confirm the highly crystalline nature of the prepared $CuFeO_2$ materials. The

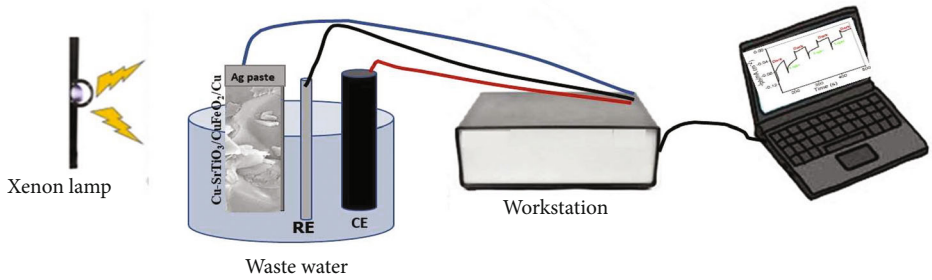

FIGURE 1: Schematic diagram of hydrogen generation from wastewater using a Cu-$SrTiO_3$/$CuFeO_2$/Cu photoelectrode.

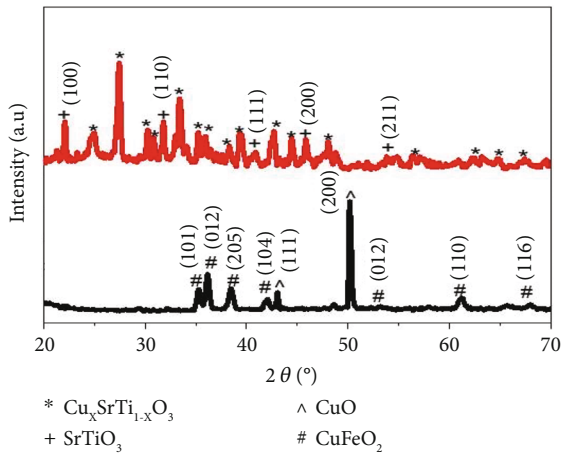

FIGURE 2: XRD of $CuFeO_2$ (black curve) and $SrTiO_3$ and $Cu_XSrTi_{1-X}O_3$ (red curve).

XRD for the STO is shown in Figure 2 (red curve). The characteristic peaks located at 22.09°, 31.88°, 41°, 45.83°, and 53.83° matched with the growth directions (100), (110), (111), (200), and (211), respectively. These characteristic peaks confirm the highly crystalline nature of the prepared perovskite materials, STO. Moreover, these peaks are matched with the previous studies. There are additional peaks for $Cu_xSrTi_{1-x}O_3$; these peaks are related to the formation of these materials under the incorporation of Cu inside the chemical structure of STO. These additional peaks are matched with the previous studies.

The oxidation states and chemical environment of components in Cu-SrTiO3 were determined using XPS. The XPS survey spectrum of Cu-$SrTiO_3$ is featured in Figure 3(a), which displays the different elements and their BE. The XPS plot comprises Cu 2p, O1s, Ti 2p, C 1s, and Sr 3d5 at 932.71, 531.26, 459.17, 283.25, and 135.83 eV, respectively. The above findings suggest forming Cu-$SrTiO_3$ thin films through the solvothermal method. Figures 3(b)–3(e) show elements of a Cu-SrTiO3 sample for O1s, Cu 2p, Sr3d, and Ti 2p, respectively. Binding energy peaks for O1s were observed at 531.26, 531.8, and 528.4 eV, which correlate to various chemical states of oxygen. Due to the existence of Sr-O and Ti-O bonds in the $SrTiO_3$ crystal lattice, the O1s XPS signal attributed to the oxygen crystal lattice was detected at 528.4 eV. Surface oxygen was assigned a peak position of 531.8 eV due to hydroxyl groups [26, 27]. On the other hand, the peak at 531.26 eV was attributable to a surface-coordinated water molecule. Figure 3(c) exhibits two significant peaks at around 932.6 and 952.4 eV that may be attributed to Cu2p3/2 and Cu 2p1/2, respectively, indicating that the synthesized material has a monovalent copper cation (Cu+). From Figure 3(d), the Sr 3d5/2 peaks at 134.04 eV and the Sr3d 3/2 peaks at 135.65 eV. As well, Ti2p peaks at 458.17 eV and 464.19 eV are illustrated in Figure 3(e).

The surface types of Fe, Cu, O, and C atoms in $CuFeO_2$/Cu are shown in the survey X-ray photoelectron spectrum in Figure 3(f), which displays the different elements and their corresponding binding energies (BE). The XPS plot comprises Cu2p, Fe2p, O1s, and C1s at 932.61, 711.25, 530.98, and 285.0 eV, respectively. The above findings suggest that the $CuFeO_2$/Cu thin film is produced through the combustion approach.

3.1.2. SEM and TEM Studies. In Figure 4(a), the design of a homogenous highly crystalline surface is seen. The crystals are compacted and connected high together on one surface. The formed nano-/microparticle for the perovskite materials is expected to have high optical properties. The significant roughness and minimum porousness of the Cu-$SrTiO_3$/$CuFeO_2$/Cu surface qualify it for absorbing light in many directions in an area of 1531.9* 1589 nm, as drawn with the ImageJ program (Figure 4(b)). The SEM of the $CuFeO_2$/Cu thin film is presented in Figure 4(c). It could be seen that the highly crystalline polyhedral $CuFeO_2$/Cu delafossite thin film is free of cracks with a smooth surface. This surface is used as a substrate for the deposition of the Cu-$SrTiO_3$ materials.

The TEM image of Cu-$SrTiO_3$/$CuFeO_2$/Cu is shown in Figure 4(d). This figure reveals the nano-/microstructured morphology of Cu-$SrTiO_3$/$CuFeO_2$ with an average crystalline particle size of 200 nm.

3.1.3. Optical Analyses. The optical characteristics of the prepared Cu-$SrTiO_3$/$CuFeO_2$ and $CuFeO_2$ are shown in Figure 5(a). The refraction of $CuFeO_2$ is higher than that of Cu-$SrTiO_3$/$CuFeO_2$, indicating that the absorption intensity is increasing, in which the electron transition is the main factor for peak formation in the UV, Vis, and near IR regions [28–31].

The $CuFeO_2$ and Cu-$SrTiO_3$/$CuFeO_2$ bandgap (Eg) values of 1.4 and 1.26 eV, respectively, show an improvement in optical characteristics (Figure 5(b)). The Kubelka-Munk equation

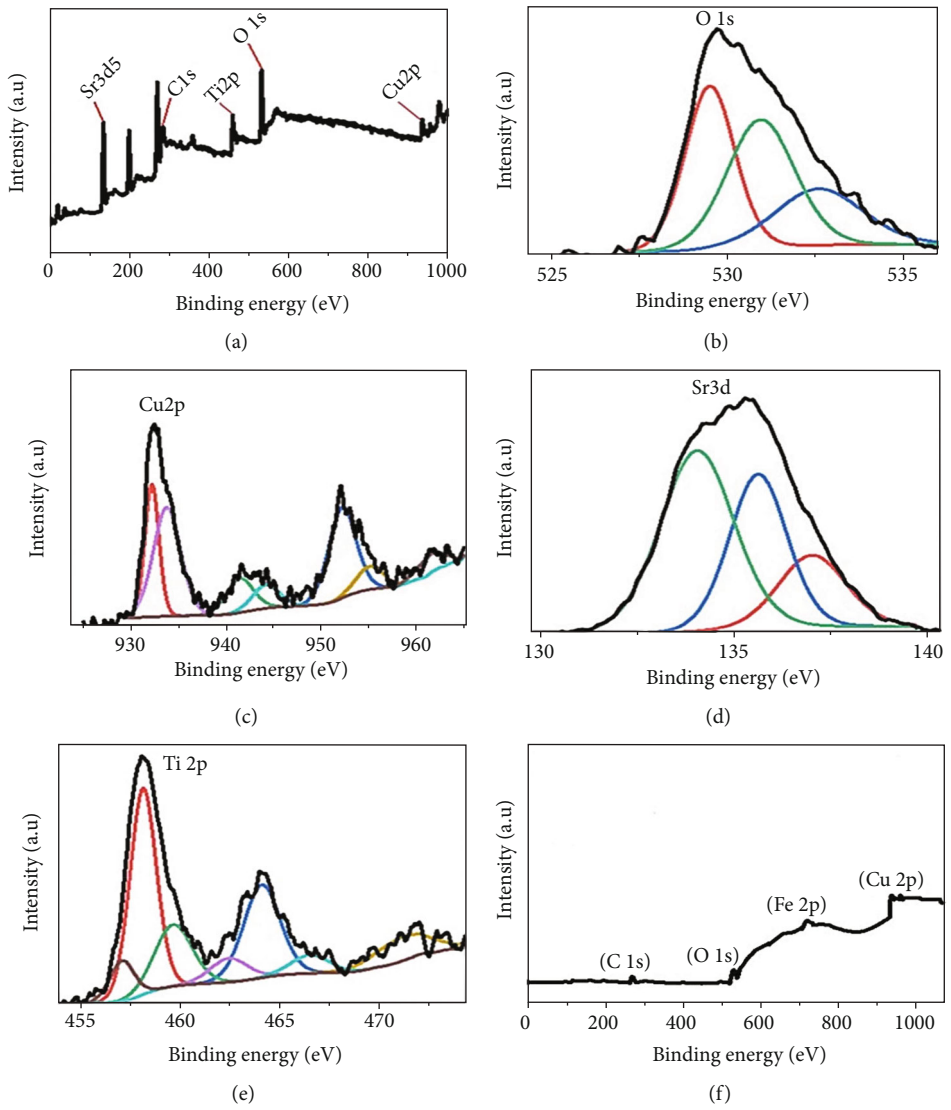

Figure 3: XPS spectra of survey spectra of (a) Cu-$SrTiO_3$, (b) O1s, (c) Cu2p, (d) Sr3d, (e) Ti2p, and (f) survey spectra of $CuFeO_2$.

was used to obtain the Eg value, where S and K are the scattering and absorption coefficients, respectively; R is the diffuse reflectance; and $F(R)$ is the Kubelka-Munk function [32].

$$\frac{K}{s} = \frac{(1 - R_\infty)^2}{2R_\infty} \equiv F(R_\infty). \quad (1)$$

3.2. Photoelectrochemical Activity. In the presence of a Xenon lamp (Newport, 66926-500HX-R07), the photoelectrochemical performance of the constructed electrode Cu-$SrTiO_3$/$CuFeO_2$/Cu for hydrogen generation is measured. The electrochemical workstation used for the measurements is CHI660E. The relationship between voltage and current density is revealed in Figure 6(a). It appears that the Cu-$SrTiO_3$/$CuFeO_2$/Cu electrode served as a photocathode for the formation of H_2 gas. Figure 6(a) shows that when exposed to light, the resultant current density (J_{ph}) is 1.292 mA.cm^{-2} at 0.5 V. The result of light intensity on the prepared photoelectrode is shown in Figures 6(a) and 6(b). When the light intensity is increased from 25 to 100 mW.cm^{-2}, the produced J_{ph} values increase from -1.02 to -1.292 mA.cm^{-2}. The J_{ph} rises with increasing light intensity owing to enhanced electron-hole pair production [33, 34]. The generated current is directly proportional to the amount of light absorbed. Because J_{ph} indicates the current density generated in the cell as a result of water splitting, it can also measure the rate of hydrogen generation from sanitation water.

As seen in Equation (2), the number of photons (N) is directly proportional to the intensity of light (P) [35]. This equation is also affected by other parameters including wavelength (λ), Planck constant (h), and light velocity (c). Applying this equation, the N per second is changed from photon/s under light intensity from 25 to 100, and mW·cm^{-2} is changed from 2×10^{21} to 8×10^{21} photon/s, respectively.

$$N = \frac{\lambda P}{hc}. \quad (2)$$

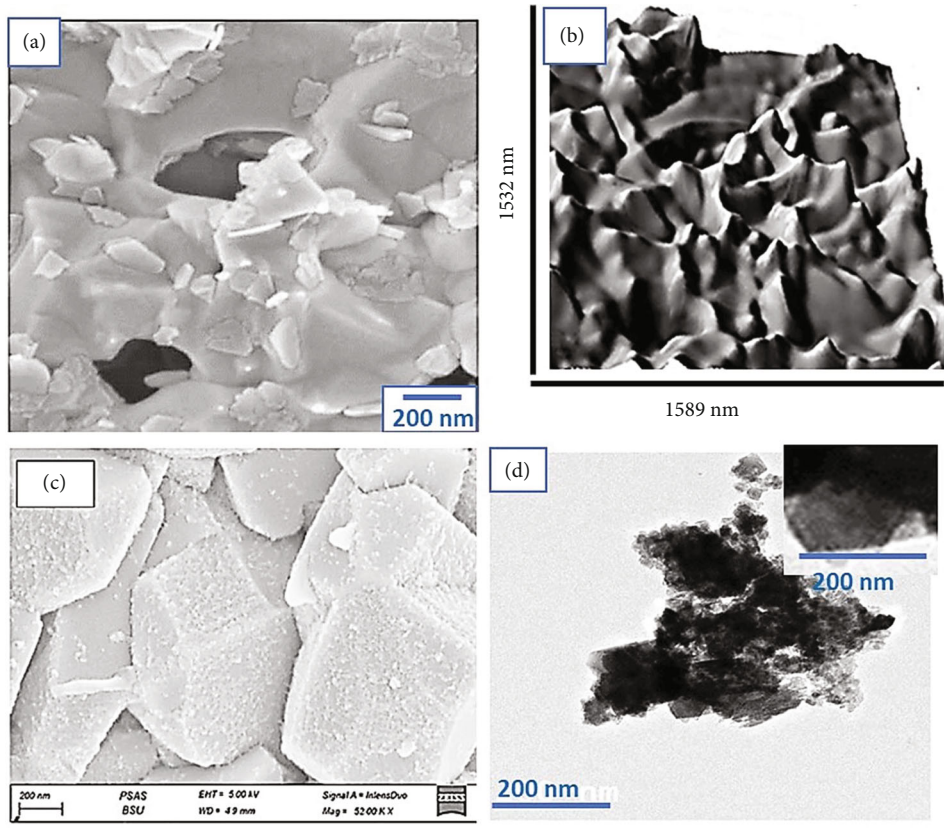

Figure 4: (a) SEM image of Cu-$SrTiO_3$/$CuFeO_2$/Cu, (b) the roughness by using the modeling program (ImageJ), (c) SEM image of $CuFeO_2$/Cu, and (d) TEM of Cu-$SrTiO_3$/$CuFeO_2$/Cu.

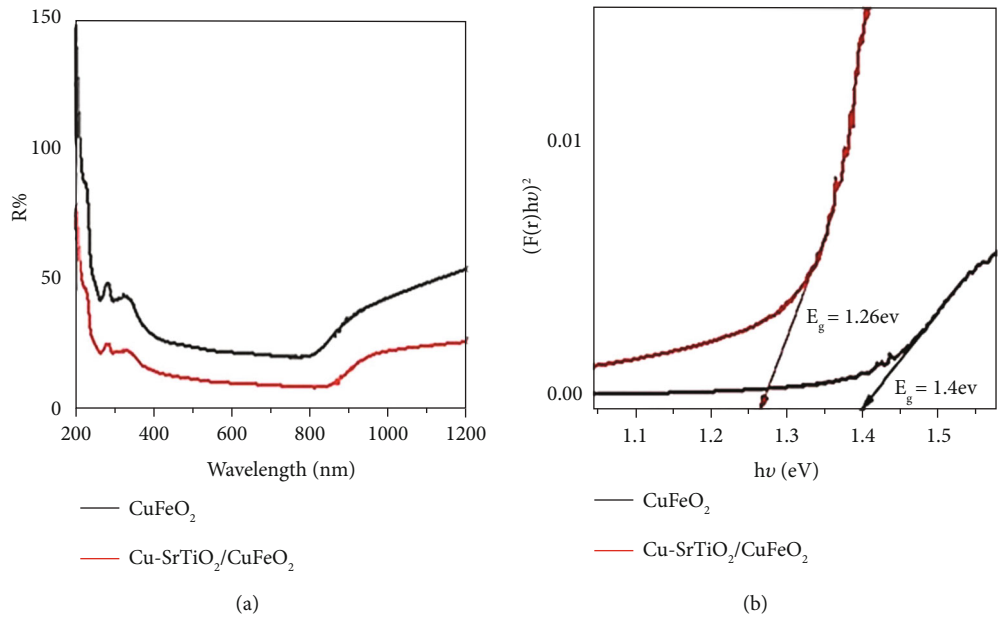

Figure 5: Optical analyses: (a) reflectance and (b) bandgap of Cu-$SrTiO_3$/$CuFeO_2$ and $CuFeO_2$.

The stability of the prepared Cu-$SrTiO_3$/$CuFeO_2$/Cu photoelectrode was investigated, as shown in Figure 7(a). The relationship between time and the generated J_{ph} value is discussed, and the produced J_{ph} value under light and dark chopping is steady with time (500 s) at around -0.11 mA.cm^{-2}. According to the figure, the electrode has good stability and high light sensitivity. The variation in J_{ph} values across on- and off-chopped light is clearly visible.

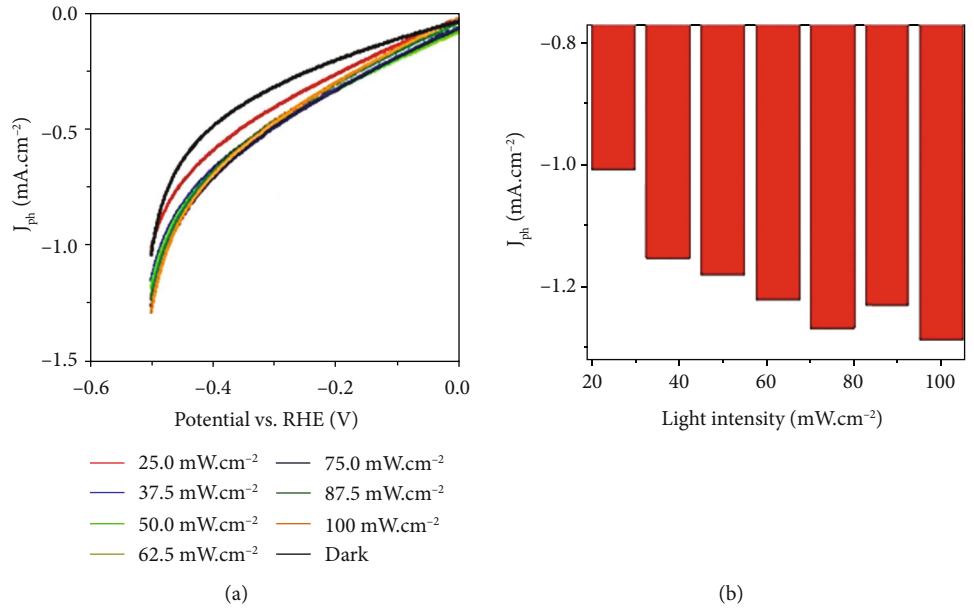

FIGURE 6: (a) Current-voltage relation by the effect of light intensity and (b) the produced J_{ph} values at -0.5 V for the prepared Cu-$SrTiO_3$/$CuFeO_2$/Cu photoelectrode.

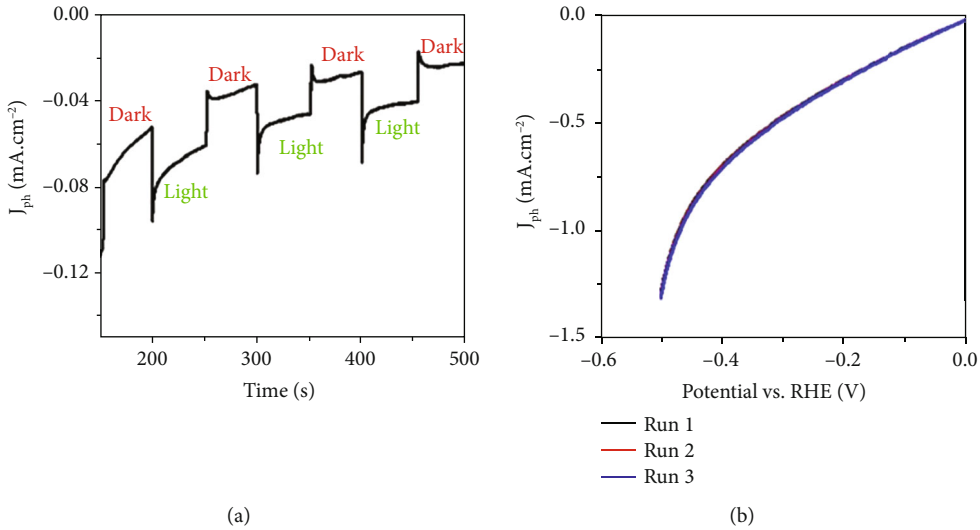

FIGURE 7: (a) The dark/light chopping current and (b) reproducibility for Cu-$SrTiO_3$/$CuFeO_2$/Cu photoelectrode.

The remarkable influence of light on the electrode confirms the electrode's high sensitivity to light. Figure 7(b) depicts the repeatability of the electrode over two runs, with the voltage-current relationship exhibiting similar performance through four runs. This repeatability has been tested at 25°C and under natural light.

The temperature effect on the Cu-$SrTiO_3$/$CuFeO_2$/Cu photoelectrode for hydrogen generation because of water splitting is revealed in Figure 8(a), where the J_{ph} rises from -1.25 to -1.91 mA.cm^{-2} as the temperature increases from 30 to 70°C, correspondingly. The overall rise in J_{ph} values represents the rate of the reaction, which correlates to the rate of hydrogen generation [2, 36]. The produced J_{ph} values at various temperatures are mentioned in Figure 8(b). Relying on particle collision and the rate of water splitting, the activation energy (Ea) could be determined using the Arrhenius equation, Equation (3), where k, R, T, and A are the rate, universal gas, absolute temperature, and Arrhenius constants, respectively [34]. The Ea value defines the degree of reaction occurrence [37–39].

$$k = Ae^{-Ea/RT}. \quad (3)$$

Figure 8(c) shows that the slope values of the relationship J_{ph} and 1/T yield the Ea value. For the Cu-$SrTiO_3$/$CuFeO_2$/Cu photoelectrode, the Ea value is 14.144 kJ mol^{-1}.

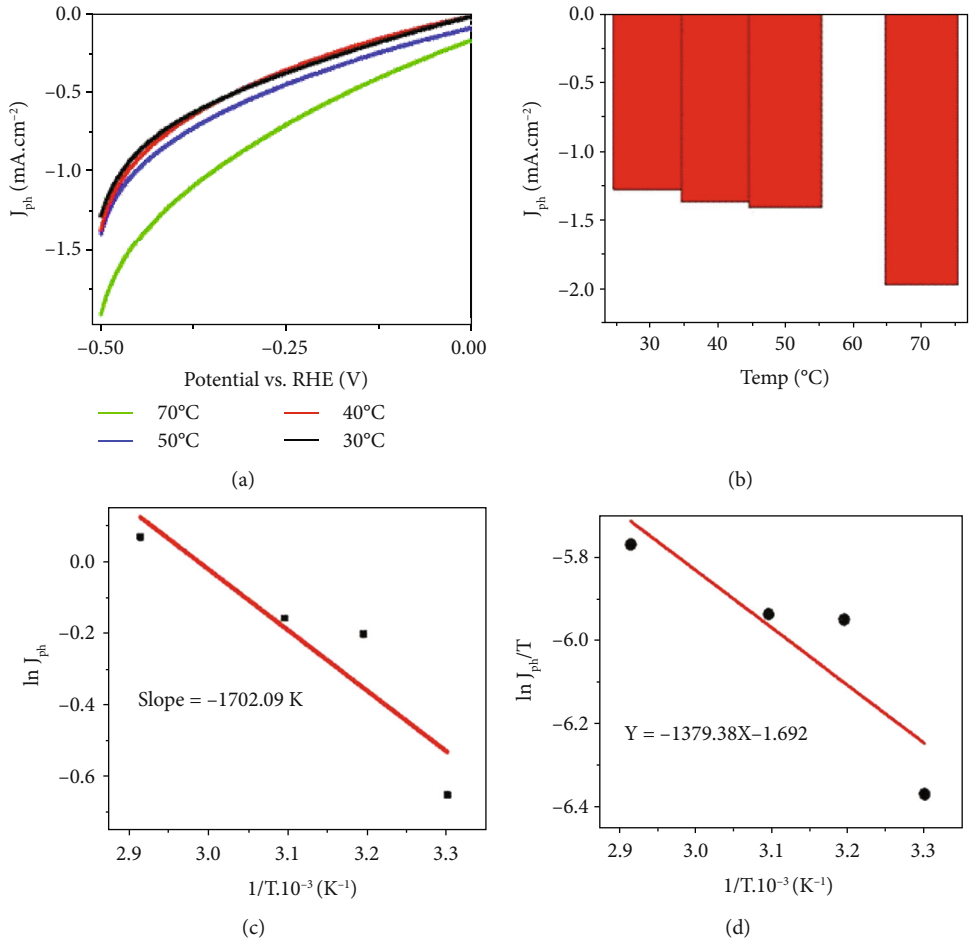

Figure 8: (a) The temperature effect and (b) the produced J_{ph} values at -0.5 V. (c) Arrhenius and (d) Eyring relations for Cu-$SrTiO_3$/$CuFeO_2$/Cu photoelectrode.

When analyzed with previously published results for different photocatalysts, the Ea value for this electrode is exceptionally low. As a result of the water-splitting reaction, the synthesized electrode is effective for H_2 evolution. Similarly, utilizing the Boltzmann constant (kB) and the Planck constant (h), the Eyring equation (4), maybe get the enthalpy (H^*) and entropy (S^*)

$$k = T.\frac{\mathrm{kB}}{h}.e^{\Delta S/R}.e^{-\Delta H/\mathrm{RT}}. \quad (4)$$

To determine the ΔH^* and ΔS^* values, slope and intercept from Figure 8(d), respectively, are used. The ΔH value of Cu-$SrTiO_3$/$CuFeO_2$/Cu photoelectrode is 11.46 kJ·mol^{-1}, while ΔS^*value is 34.9 kJ^{-1}·mol^{-1}.

The photocurrent produced as a result of photon energy is defined as the incident photon-to-current conversion efficiency (IPCE). The wavelength value can be used to determine it. Equation (5) is used to compute the IPCE [18, 40–42].

$$\mathrm{IPCE} = \frac{1240}{\lambda(\mathrm{nm})}\frac{Jph\ (\mathrm{mA/cm^2})}{P\ (\mathrm{mW/cm^2})} \times 100(\%). \quad (5)$$

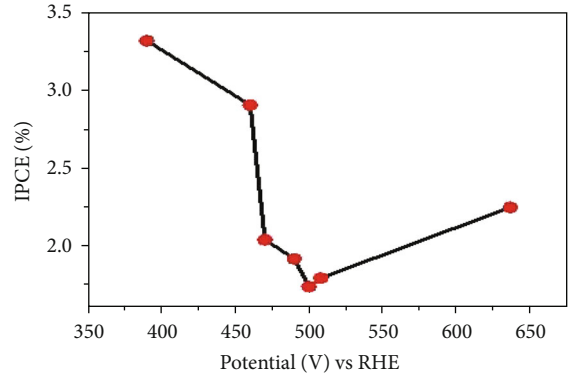

Figure 9: The IPCE for Cu-$SrTiO_3$/$CuFeO_2$/Cu photoelectrode.

In Figure 9, the IPCE is calculated at a light intensity of 100 mW.cm^2 and a temperature of 30°C. At 390 nm, the electrode has the optimum IPCE of 3.31%. This value is reduced by raising the wavelength to 500 nm, then rising until it reaches 636 nm. The IPCE value is obtained from the impact of the electrode's photocatalytic ability for sanitation water splitting without the presence of an additional

Table 1: Comparing the current study to the previous literature for H_2 generation reaction.

Photoelectrode	Applied voltage (V)	J_{ph} (mA/cm^2)	Electrolyte	Light source	IPCE% (390 nm)
CuO-C/TiO_2 [44]	-0.5	0.001	Glycerol	300 W xenon lamp	—
CuO nanowire [45]	-0.5	1.5	Na_2SO_4	Simulated AM1.5 illumination CuO	—
ZnO/TiO_2/FeOOH [46]	0.8	1.59	$Na_2S_2O_3$	A 150 W xenon lamp	—
SnO_2/TiO_2 [47]	0.6	0.4	$Na_2S_2O_3$	1 Sun (100 mW cm^{-2})	—
$BiFeO_3$ [48]	1.6	0.1	NaOH	1 sun (AM 1.5G solar spectrum)	0.21
PrFeO [49]	-0.6	0.130	Na_2SO_4	Simulated sunlight	—
Poly(3-aminobenzoic acid) frame [50]	1.6	1.2	H_2SO_4	150 W xenon lamb	—
$CuFeO_2$ [50]	0.81	0.3	1 M NaOH	1 sun illumination	—
$CuFeO_2$ [50]	0.9	1.25	1 M NaOH	1 sun illumination	—
$CuFe_2O_4$ [51]	1.1	0.04	0.1 M NaOH	1 sun illumination	—
$CuFe_2O_4$ [52]	1.05	1.82	1 M NaOH	1 sun illumination	—
Cu-$SrTiO_3$/$CuFeO_2$/Cu	-0.5	-1.91	Sewage water	Simulated sunlight	3.31

electrolyte. As a result, the device converts sanitation water to H_2 with more efficiency than earlier studies have shown.

Equation (6) was used to determine the amount of H_2 moles [43], where F is the Faraday constant and dt is the time change. Production of H_2 increases with time, corresponding to 10 ml/h for the sample with a dimension of 20 cm^2 for hydrogen production from a photoelectrode. Moreover, Table 1 illustrates a comparison of our study with previous literature.

$$H_2 \text{ mole} = \int_0^t J_{ph} \cdot \frac{dt}{F}. \quad (6)$$

4. Conclusions

A photodetector made of Cu-$SrTiO_3$/$CuFeO_2$/Cu was used to produce hydrogen gas from sanitation water. XRD analysis confirmed the formation of perovskite materials, including $SrTiO_3$ and $Cu_xSrTi_{1-x}O_3$, as well as $CuFeO_2$ and CuO. SEM analysis confirmed that the materials were highly crystalline with small surface pores. The materials' excellent optical properties were confirmed by their small bandgap values of 1.4 and 1.26 eV for $CuFeO_2$ and Cu-$SrTiO_3$/$CuFeO_2$, respectively. During hydrogen generation, J_{ph} values were significantly enhanced under light compared to dark conditions. Moreover, increasing the light intensity from 25 to 100 mW/cm^2 increased the produced J_{ph} values from -1.02 to -1.292 mA/cm^2. Temperature also had a significant effect, with the J_{ph} rising from -1.25 to -1.91 mA/cm^2 as the temperature increased from 30 to 70°C. The study measured various thermodynamic parameters related to the rate of hydrogen gas evolution, including an Ea value of 14.14 kJ mol^{-1} and H^* and S^* values of 11.46 kJ mol^{-1} and 34.9 kJ mol^{-1}, respectively. These findings are promising for H_2 gas fuel production, and the team plans to design a prototype of cells that can directly convert wastewater into H_2 gas fuel.

Data Availability

The authors confirm that the data supporting the findings of this study are available within the article.

Conflicts of Interest

The authors declare that they have no conflicts of interest.

Authors' Contributions

The methodology was prepared by Aya Ahmed. Formal analysis was done by Ashour M. Ahmed, Ahmed A. Abdel-Khaliek, Mohamed Shaban, Ahmed Adel A. Abdelazeez, and Mohamed Rabia. The investigation was performed by Ahmed Adel A. Abdelazeez and Mohamed Rabia. Supervision was implemented by Ahmed A. Abdel-Khaliek, Mohamed Shaban, and Mohamed Rabia. Writing—original draft preparation—was done by Aya Ahmed and Mohamed Rabia. Writing, which includes review and editing, was performed by Ahmed A. Abdel-Khaliek, Ahmed Adel A. Abdelazeez, and Mohamed Rabia. Open Access funding is enabled and organized by Carolinas 2023.

Acknowledgments

This paper is based on work supported by the Science, Technology & Innovation Funding Authority (STDF) under a grant given to Aya Ahmed, with the project number 44746.

References

[1] Y. Liu, C. H. Liu, T. Debnath et al., "Silver nanoparticle enhanced metal-organic matrix with interface-engineering for efficient photocatalytic hydrogen evolution," *Nature Communications*, vol. 14, no. 1, p. 541, 2023.

[2] H. Xie, Z. Zhao, T. Liu et al., "A membrane-based seawater electrolyser for hydrogen generation," *Nature*, vol. 612, no. 7941, pp. 673–678, 2022.

[3] G. Lopez, L. Santamaria, A. Lemonidou et al., "Hydrogen generation from biomass by pyrolysis," *Nature Reviews Methods Primers*, vol. 2, no. 1, 2022.

[4] Z. Li, G. Huang, Y. Wang, C. Lu, H. Huang, and J. Kou, "Pyroelectric effects in CdS phase junctions for dual-enhanced photocatalytic hydrogen production," *Catalysis Science & Technology*, vol. 13, no. 8, pp. 2559–2565, 2023.

[5] S. Masudy-Panah, R. Siavash Moakhar, C. S. Chua, A. Kushwaha, and G. K. Dalapati, "Stable and efficient CuO based photocathode through oxygen-rich composition and au-Pd nanostructure incorporation for solar-hydrogen production," *ACS Applied Materials and Interfaces*, vol. 9, no. 33, pp. 27596–27606, 2017.

[6] X. F. Shi, X. Y. Xia, G. W. Cui et al., "Multiple exciton generation application of PbS quantum dots in /graphene oxide for enhanced photocatalytic activity," *Applied Catalysis B: Environmental*, vol. 163, pp. 123–128, 2015.

[7] M. Shaban, M. Rabia, A. M. A. El-Sayed, A. Ahmed, and S. Sayed, "Photocatalytic properties of PbS/graphene oxide/polyaniline electrode for hydrogen generation," *Scientific Reports*, vol. 7, no. 1, article 14100, 2017.

[8] J. Liu, Q. Yuan, W. Huang, and X. Song, "A novel nanoporous mg-Li material for efficient hydrogen generation," *Journal of Magnesium and Alloys*, vol. 10, no. 11, pp. 3054–3063, 2022.

[9] J. Davies, S. P. du Preez, and D. G. Bessarabov, "On-Demand Hydrogen Generation by the Hydrolysis of Ball-Milled Aluminum–Bismuth–Zinc Composites," *Materials*, vol. 15, no. 3, p. 1197, 2022.

[10] I. Mesquita, L. Andrade, and A. Mendes, "Perovskite solar cells: materials, configurations and stability," *Renewable and Sustainable Energy Reviews*, vol. 82, pp. 2471–2489, 2018.

[11] C. Xie, C. K. Liu, H. L. Loi, and F. Yan, "Perovskite-based phototransistors and hybrid photodetectors," *Advanced Functional Materials*, vol. 30, no. 20, article 1903907, 2020.

[12] F. Gu, S. Ye, Z. Zhao et al., "Improving performance of lead-free formamidinium tin triiodide perovskite solar cells by tin source purification," *Solar RRL.*, vol. 2, no. 10, article 1800136, 2018.

[13] S. Y. Tsai, C. C. Lin, C. T. Yu et al., "Screen-printable silver paste material for semitransparent and flexible metal–semiconductor–metal photodetectors with liquid-phase procedure," *Nanomaterials*, vol. 12, no. 14, p. 2428, 2022.

[14] X. Yu, T. J. Marks, and A. Facchetti, "Metal oxides for optoelectronic applications," *Nature Materials*, vol. 15, no. 4, pp. 383–396, 2016.

[15] B. Wang, A. Thukral, Z. Xie et al., "Flexible and stretchable metal oxide nanofiber networks for multimodal and monolithically integrated wearable electronics," *Nature Communications*, vol. 11, no. 1, pp. 1–11, 2020.

[16] M. M. Abdelhamied, A. Atta, A. M. Abdelreheem, A. T. M. Farag, and M. M. El Okr, "Synthesis and optical properties of PVA/PANI/ag nanocomposite films," *Journal of Materials Science: Materials in Electronics*, vol. 31, no. 24, pp. 22629–22641, 2020.

[17] J. M. Yu, J. Lee, Y. S. Kim et al., "High-performance and stable photoelectrochemical water splitting cell with organic-photoactive-layer-based photoanode," *Nature Communications*, vol. 11, no. 1, p. 5509, 2020.

[18] S. D. Tilley, "Recent advances and emerging trends in photoelectrochemical solar energy conversion," *Advanced Energy Materials*, vol. 9, no. 2, article 1802877, 2019.

[19] J. Shi and L. Guo, "ABO_3-based photocatalysts for water splitting," *Progress in Natural Science: Materials International*, vol. 22, no. 6, pp. 592–615, 2012.

[20] A. Kolivand and S. Sharifnia, "Enhanced photocatalytic hydrogen evolution from water splitting by Z-scheme CdS/$BiFeO_3$ heterojunction without using sacrificial agent," *International Journal of Energy Research*, vol. 45, no. 2, pp. 2739–2752, 2021.

[21] Y. Guo, G. Liu, Z. Li, Y. Lou, J. Chen, and Y. Zhao, "Stable lead-free $(CH_3NH_3)_3Bi_2I_9$ perovskite for photocatalytic hydrogen generation," *ACS Sustainable Chemistry and Engineering*, vol. 7, no. 17, pp. 15080–15085, 2019.

[22] T. Bin Song, T. Yokoyama, C. C. Stoumpos et al., "Importance of reducing vapor atmosphere in the fabrication of tin-based perovskite solar cells," *Journal of the American Chemical Society*, vol. 139, no. 2, pp. 836–842, 2017.

[23] O. Malinkiewicz, C. Roldán-Carmona, A. Soriano et al., "Metal-oxide-free methylammonium lead iodide perovskite-based solar cells: the influence of organic charge transport layers," *Advanced Energy Materials*, vol. 4, no. 15, article 1400345, 2014.

[24] D. B. Mitzi, "Organic-inorganic perovskites containing trivalent metal halide layers: the templating influence of the organic cation layer," *Inorganic Chemistry*, vol. 39, no. 26, pp. 6107–6113, 2000.

[25] X. Qiu, M. Liu, K. Sunada, M. Miyauchi, and K. Hashimoto, "A facile one-step hydrothermal synthesis of rhombohedral $CuFeO_2$ crystals with antivirus property," *Chemical Communications*, vol. 48, no. 59, pp. 7365–7367, 2012.

[26] R. Lin, Z. Li, D. I. Abou El Amaiem et al., "A general method for boosting the supercapacitor performance of graphitic carbon nitride/graphene hybrids," *Journal of Materials Chemistry A*, vol. 5, no. 48, pp. 25545–25554, 2017.

[27] M. H. Patel, T. K. Chaudhuri, V. K. Patel, T. Shripathi, U. Deshpande, and N. P. Lalla, "Dip-coated PbS/PVP nanocomposite films with tunable band gap," *RSC Advances*, vol. 7, no. 8, pp. 4422–4429, 2017.

[28] S. A. Hameed and H. A. Ewais, "Kinetics and mechanism of the redox reaction between malachite green and iron(III) in aqueous and micellar media," *Transition Metal Chemistry*, vol. 39, no. 2, pp. 199–204, 2014.

[29] H. A. Ewais, S. A. Ahmed, and A. A. Abdel-Khalek, "Kinetics and mechanism of oxidation of chromium(III)-guanosine 5-monophosphate complex by periodate," *Journal of the Chinese Chemical Society*, vol. 51, no. 4, pp. 713–718, 2004.

[30] H. A. Ewais, F. D. Al-Otaibi, and A. A. Abdel-Khalek, "Kinetics and mechanism of oxidation of iminodiacetatochromium(III) by periodate," *Inorganic Reaction Mechanisms*, vol. 6, pp. 39–47, 2006.

[31] H. A. Ewais, F. D. Dahman, and A. A. Abdel-Khalek, "Inner-sphere oxidation of ternary iminodiacetatochromium(III) complexes involving DL-valine and L-arginine as secondary ligands. Isokinetic relationship for the oxidation of ternary iminodiacetato-chromium(III) complexes by periodate," *Chemistry Central Journal*, vol. 3, no. 1, 2009.

[32] D. V. Wellia, D. Nofebriani, N. Pratiwi, and S. Safni, "Synthesis of porous N-doped TiO2 by using peroxo sol-gel method for photocatalytic reduction of cd(II)," *Bulletin of Chemical Reaction Engineering & Catalysis*, vol. 17, no. 1, pp. 103–112, 2022.

[33] H. S. H. Mohamed, M. Rabia, X. G. Zhou et al., "Phase-junction Ag/TiO_2 nanocomposite as photocathode for H_2

generation," *Journal of Materials Science & Technology.*, vol. 83, pp. 179–187, 2021.

[34] X. Xiao, C. Engelbrekt, M. Zhang et al., "A straight forward approach to electrodeposit tungsten disulfide/poly(3,4-ethylenedioxythiophene) composites onto nanoporous gold for the hydrogen evolution reaction," *Applied Surface Science*, vol. 410, pp. 308–314, 2017.

[35] M. M. Abdelhamied, M. M. Ghobashy, N. M. A. Hadia et al., "Chemical deposition of Ag and Ag_2O on grafting film of PET-COOH by photografting polymerization for optoelectronic application," *Journal of Materials Science: Materials in Electronics*, vol. 34, pp. 1–11, 2023.

[36] X. Zhang, X. Zhao, P. Zhu et al., "Electrochemical oxygen reduction to hydrogen peroxide at practical rates in strong acidic media," *Nature Communications*, vol. 13, no. 1, p. 2880, 2022.

[37] A. Helmy, M. Rabia, M. Shaban, A. M. Ashraf, S. Ahmed, and A. M. Ahmed, "Graphite/rolled graphene oxide/carbon nanotube photoelectrode for water splitting of exhaust car solution," *International Journal of Energy Research*, vol. 44, no. 9, pp. 7687–7697, 2020.

[38] J. M. Serra, J. F. Borrás-Morell, B. García-Baños et al., "Hydrogen production via microwave-induced water splitting at low temperature," *Energy*, vol. 5, no. 11, pp. 910–919, 2020.

[39] N. M. A. Hadia, A. Hajjiah, A. M. Elsayed et al., "Bunch of grape-like shape PANI/Ag_2O/Ag nanocomposite photocatalyst for hydrogen generation from wastewater," *Adsorption Science & Technology.*, vol. 2022, pp. 1–11, 2022.

[40] J. Tian, Q. Xue, Q. Yao, N. Li, C. J. Brabec, and H. L. Yip, "Inorganic halide perovskite solar cells: progress and challenges," *Advanced Energy Materials*, vol. 10, no. 23, article 2000183, 2020.

[41] Z. Zhan, F. Grote, Z. Wang et al., "Degenerating plasmonic modes to enhance the performance of surface plasmon resonance for application in solar energy conversion," *Advanced Energy Materials*, vol. 5, no. 24, article 1501654, 2015.

[42] H. Baig, H. Kanda, A. M. Asiri, M. K. Nazeeruddin, and T. Mallick, "Increasing efficiency of perovskite solar cells using low concentrating photovoltaic systems," *Sustainable Energy & Fuels*, vol. 4, no. 2, pp. 528–537, 2020.

[43] N. M. A. Hadia, M. A. H. Khalafalla, F. M. A. Salam et al., "Conversion of sewage water into H_2 gas fuel using hexagonal nanosheets of the polyaniline-assisted deposition of PbI_2 as a nanocomposite photocathode with the theoretical qualitative Ab-initio calculation of the H_2O splitting," *Polymers*, vol. 14, no. 11, p. 2148, 2022.

[44] X. Huang, M. Zhang, R. Sun, G. Long, Y. Liu, and W. Zhao, "Enhanced hydrogen evolution from CuO_x-C/TiO_2 with multiple electron transport pathways," *PLoS One*, vol. 14, no. 4, p. e0215339, 2019.

[45] J. Li, X. Jin, R. Li et al., "Copper oxide nanowires for efficient photoelectrochemical water splitting," *Applied Catalysis B: Environmental*, vol. 240, pp. 1–8, 2019.

[46] N. M. A. Hadia, A. A. A. Abdelazeez, M. Alzaid et al., "Converting sewage water into H_2 fuel gas using Cu/CuO nanoporous photocatalytic electrodes," *Materials*, vol. 15, no. 4, p. 1489, 2022.

[47] B. D. Sherman, D. L. Ashford, A. M. Lapides, M. V. Sheridan, K. R. Wee, and T. J. Meyer, "Light-driven water splitting with a molecular electroassembly-based core/shell photoanode," *Journal of Physical Chemistry Letters.*, vol. 6, no. 16, pp. 3213–3217, 2015.

[48] G. Liu, S. K. Karuturi, H. Chen et al., "Enhancement of the photoelectrochemical water splitting by perovskite $BiFeO_3$*via* interfacial engineering," *Solar Energy*, vol. 202, pp. 198–203, 2020.

[49] E. Freeman, S. Kumar, S. R. Thomas, H. Pickering, D. J. Fermin, and S. Eslava, "$PrFeO_3$ photocathodes prepared through spray pyrolysis," *ChemElectroChem*, vol. 7, no. 6, pp. 1365–1372, 2020.

[50] K. D. Modibane, N. J. Waleng, K. E. Ramohlola et al., "Poly(3-aminobenzoic acid) decorated with cobalt zeolitic benzimidazolate framework for electrochemical production of clean hydrogen," *Polymers*, vol. 12, no. 7, pp. 1–14, 2020.

[51] M. I. Díez-García, T. Lana-Villarreal, and R. Gómez, "Study of copper ferrite as a novel photocathode for water reduction: improving its photoactivity by electrochemical pretreatment," *ChemSusChem*, vol. 9, no. 12, pp. 1504–1512, 2016.

[52] S. Park, J. H. Baek, L. Zhang et al., "Rapid flame-annealed $CuFe_2O_4$ as efficient photocathode for photoelectrochemical hydrogen production," *ACS Sustainable Chemistry and Engineering*, vol. 7, no. 6, pp. 5867–5874, 2019.